Enhanced photocatalytic activity of Bi_2WO_6 loaded with Ag nanoparticles under visible light irradiation

Jia Ren [a], Wenzhong Wang [a,*], Songmei Sun [a], Ling Zhang [a], Jiang Chang [b]

[a] State Key Laboratory of High Performance Ceramics and Superfine Microstructure, Shanghai Institute of Ceramics, Chinese Academy of Sciences, 1295 Dingxi Road, Shanghai 200050, PR China
[b] Biomaterials and Tissue Engineering Research Center, Shanghai Institute of Ceramics, Chinese Academy of Sciences, 1295 Dingxi Road, Shanghai 200050, PR China

ARTICLE INFO

ABSTRACT

Ag-loaded Bi_2WO_6 nanoparticles were prepared via a facile alcohol-thermal process in ethylene alcohol system. The products were characterized by XRD, TEM, HRTEM and energy-dispersed X-ray (EDX) microanalysis. The results revealed that it was the metallic Ag deposited on Bi_2WO_6, which was further confirmed by the surface plasmon absorption band existed in the UV–vis absorption spectrum. Compared with pure Bi_2WO_6, Ag-loaded Bi_2WO_6 photocatalysts exhibited significantly enhanced photocatalytic activity in inactivating E. coli, a Gram-negative bacterium, and S. epidermidis, a Gram-positive bacterium under visible light irradiation ($\lambda > 420$ nm). The influence of the content of silver on the catalytic activity of Bi_2WO_6 photocatalyst has been investigated. The results concerning the effect of silver on the catalytic activity of Bi_2WO_6 photocatalyst revealed that the significant enhancement of photocatalytic activity can be attributed to the synergetic effects between noble metal and semiconductor component.

1. Introduction

Since photoinduced decomposition of water on TiO_2 electrodes was discovered, semiconductor-based photocatalysis has attracted extensive interest [1]. Photocatalysis is one of the most promising technologies for water purification characterized by the generation of •OH radicals and other oxidative radicals. The general process for the photocatalytic destruction of organic substances can be divided into three steps: (1) the electrons in the valence band are excited to the conduction band leaving holes in the valence band simultaneously, when the energy of the incident light is equal or higher than the band-gap of the semiconductor; (2) the photogenerated electrons and holes transfer separately to the surface of the semiconductor to be captured by the oxygen and H_2O absorbed, forming the oxidative species •OH, $O_2^{\bullet-}$, etc.; (3) the oxidative species attack the objects, resulting in the degradation of organic compounds and the inactivation of microorganisms. In the second step, the photogenerated electrons and holes may recombine before they arrived at the surface of the semiconductor, leading to the decrease of the photocatalytic activity. Therefore, the competition between the transfer and the recombination process of photogenerated electron–hole pairs is an important

factor, which limits the photocatalytic activity of photocatalysts. In recent years, many studies have been carried out to overcome the limitation, including the coupling two kinds of matching compounds [2–5], and the deposition of noble metals such as silver [6,7], gold [8,9], platinum [10,11], and palladium [12,13].

Recently, semiconductor–metal composites were designed to improve the catalytic ability inspired by the synergetic action between semiconductor and metal component. One kind of synergetic action brought by combining noble metal nanoparticles with semiconductor oxides works via facilitating the charge separation and improving the photocatalytic activity. The noble metal nanoparticles deposited on the semiconductor oxides could act as a sink for electrons and promote interfacial electron transfer process due to its high Schottky barriers at the metal–semiconductor interface [14,15]. There have been reports that noble metals such as Pt, Au or Ag deposited on semiconductor TiO_2 were achieved so as to enhance the photocatalytic activity [16–18]. Photoelectrochemical studies operated on the Au–TiO_2 composite system also exhibited enhanced photocurrent generation in virtue of the improved interfacial charge transfer [19]. Therefore, it is believed that the metal nanoparticle deposition facilitates separation of charge carriers and promotes interfacial electron transfer process. Surface plasmon resonances of noble metal particles, which can be induced by light irradiation, may also contribute to the enhanced photocatalytic activity. A plasmonic photocatalyst was proposed by Awazu et al. [20]. It was suggested that the photocatalytic behavior

of TiO_2 was greatly boosted by the enhanced near-field amplitudes of localized surface plasmon, which arisen from an Ag core covered with a silica shell.

Bi_2WO_6 has been found to possess excellent intrinsic physical and chemical properties, such as ferroelectric piezoelectricity, catalytic behavior, and non-linear dielectric susceptibility [21]. Thus, many efforts have been devoted to study the properties of Bi_2WO_6, including the catalytic property [22–25]. Previously, our group has reported the preparation, photocatalytic activity, and stability of Bi_2WO_6 in the degradation of dyes [26–28]. The results exhibited high photocatalytic activity of Bi_2WO_6 in the degradation of dye. Inspired by the disinfection by TiO_2 photocatalysts, hereby, we expected that Bi_2WO_6 may also can inactivate microorganisms via photocatalytic process thus extend the researches on Bi_2WO_6 further. Considering the synergetic effect between the noble metal and semiconductor components, for the first time Ag nanoparticles were deposited on Bi_2WO_6 nanoparticles, to further improve the photocatalytic activity of photocatalyst Bi_2WO_6. And the results demonstrated that Ag-loaded Bi_2WO_6 exhibited significantly enhanced photocatalytic activity compared with pure Bi_2WO_6 in inactivation of both *E. coli*, a Gram-negative bacterium and *S. epidermidis*, a Gram-positive bacterium.

2. Experimental

2.1. Preparation of photocatalysts

All the reagents were of analytical grade and were used without any further purification. Ag-loaded Bi_2WO_6 was synthesized by a facile alcohol-thermal process in ethylene alcohol system. In a typical procedure, 0.97 g $Bi(NO_3)_3 \cdot 5H_2O$ and 0.33 g $Na_2WO_4 \cdot 2H_2O$ were dissolved in 20 mL ethylene alcohol, respectively. A transparent solution was obtained when the two solutions were mixed together under magnetic stirring at room temperature. Then, certain amount of $AgNO_3$ (0.1 or 1.0 mmol) was added to the above solution, and the solution was still transparent. The transparent solution was added into a 50 mL Teflon-lined autoclave up to 80% of the total volume. Then the autoclave was sealed in a stainless steel tank and heated at 160 °C for 24 h. Subsequently, the reactor was cooled to room temperature naturally. The resulting samples were collected and washed with de-ionized water and dried at 60 °C in air. Ag-loaded samples with different Ag/Bi_2WO_6 molar ratios were prepared and denoted as AB-0.1 and AB-1.0 according to the molar of reagent $AgNO_3$ used in the preparation. To find the appropriate content of Ag deposition so as to achieve the best photocatalytic activity, other loading contents of $Ag–Bi_2WO_6$ samples (AB-0.05, AB-0.5, and AB-0.75, denoted according to the mmolar used of reagent $AgNO_3$ in the preparation) were prepared and the photocatalytic bactericidal activities were evaluated by the inactivation of *E. coli* under visible light irradiation. Pure Bi_2WO_6 sample denoted as AB-0 was also synthesized under the same condition to compare their photo-catalytic inactivation activities.

2.2. Characterization

The powder X-ray diffraction (XRD) patterns of the as-synthesized samples were recorded on a D/MAX 2250 V diffract-ometer (Rigaku, Japan) using monochromatized Cu Kα ($\lambda = 0.15418$ nm) radiation under 40 kV and 100 mA and with the 2θ ranging from 10° to 70°. UV–vis diffuse reflectance spectra of the samples were obtained on an UV–vis spectrophotometer (Hitachi U-3010) using $BaSO_4$ as reference. Transmission electron microscopy (TEM) and high-resolution transmission electron microscopy (HRTEM) images were obtained using a JEOL JEM-

2100F field emission electron microscope at acceleration voltage of 200 kV.

2.3. Preparation of the bacterial culture

Two types of bacteria, *E. coli*, a Gram-negative bacterium, and *S. epidermidis*, a Gram-positive bacterium, were used as model bacteria in this study. They were incubated in Lysogeny Broth (LB) medium at 37 °C for 18 h. Cells were harvested from overnight culture by centrifugation at 4000 rpm for 5 min and then washed twice with 0.9% saline.

2.4. Bactericidal activity

The bactericidal activity of the samples was evaluated by the inactivation of *E. coli* and *S. epidermidis* under visible light irradiation ($\lambda > 420$ nm). All materials used in the experiments were autoclaved at 121 °C for 40 min before use to ensure sterility. The treated cells were suspended and diluted to a cell suspension of $\sim 2 \times 10^7$ cfu/mL with 0.9% saline to remove the influence of osmotic pressure on bacterial cells. The final photocatalyst concentration was adjusted to 0.5 mg/mL. A 500 W Xe lamp was used as the light source with a UV cutoff filter ($\lambda > 420$ nm) to provide visible light irradiation. The reaction mixture was stirred with a magnetic stirrer to prevent settling of the photocatalysts. The experiments were carried out at room temperature. Before and after the experiments, an aliquot of the reaction mixture was immediately diluted with 0.9% saline and plated on LB-agar plates. The colonies were counted after incubation at 37 °C for 24 h. All of the above experiments were repeated three times and the average values were given.

3. Results and discussion

3.1. XRD analysis

The powder X-ray diffraction (XRD) patterns of the as-synthesized Ag-loaded Bi_2WO_6 samples were recorded. As shown in Fig. 1, all the diffraction peaks can be categorized into two sets. The unmarked peaks can be indexed as an orthorhombic Bi_2WO_6 corresponding to JCPDS files no. 39-0256 ($a = 5.457$ Å, $b = 16.435$ Å, and $c = 5.438$ Å), while the marked agree well with face-centered cubic Ag corresponding to JCPDS files no. 04-0783. No other peaks from possible impurities are detected. Moreover, the changes of all diffractions and lattice parameters of Bi_2WO_6 in all Ag-loaded
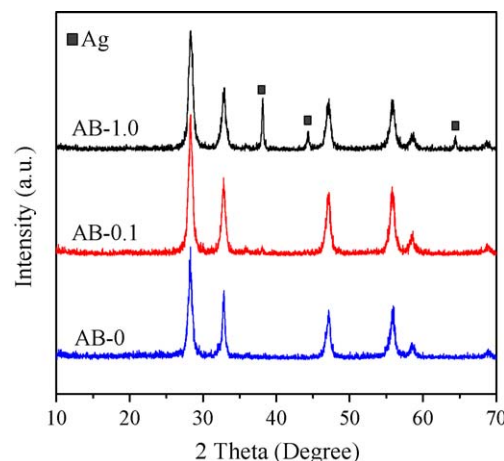

Fig. 1. XRD patterns of the Bi_2WO_6 and Ag-loaded Bi_2WO_6 samples with different silver contents.
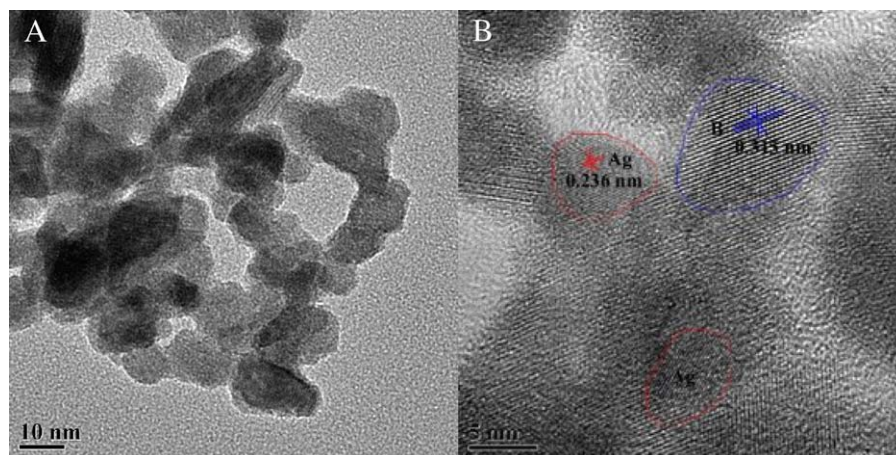
Fig. 2. TEM (A) and HRTEM (B) images Ag-loaded Bi_2WO_6 nanocomposite obtained in the presence of 0.1 mmol $AgNO_3$, where B and Ag represent Bi_2WO_6 and silver nanocrystal particles, respectively.

Bi_2WO_6 samples are not detectable, which implies that Ag did not get into the lattice of Bi_2WO_6, but on the surface.

3.2. TEM observation and energy-dispersed X-ray microanalysis

The morphology of Ag-loaded Bi_2WO_6 (AB-0.1) sample was revealed by TEM. The panoramic view shown in Fig. 2A indicates that the as-prepared sample is composed of nanoparticles with size of 10–20 nm. A HRTEM image of the same sample consisting of Ag and Bi_2WO_6 nanoparticles is shown in Fig. 2B. The distance between two fringes in B marked area is about 0.315 nm, which is close to the d spacing of (1 3 1) plane of orthorhombic Bi_2WO_6. The result is well consistent with that of XRD pattern in Fig. 1, where the peaks of (1 3 1) plane is much stronger compared with those of standard patterns. And the lattice fringes with interplanar spacing of 0.236 nm are also observed, corresponding to the (1 1 1) plane of Ag nanoparticles. The silver nanoparticles are in close contact with the Bi_2WO_6 nanoparticles, which is believed to facilitate the electron transfer between the noble metal and semiconductor [29]. In order to further confirm the existence of Ag, the areas with and without the deposited Ag were selected respectively for energy-dispersed X-ray (EDX) microanalysis. According to Fig. 3, signal corresponding to silver was detected in the area with silver deposited. The Ag peaks are not apparent in the XRD pattern of the sample AB-0.1 due to the small content of Ag contained, while clear Ag peaks of the sample AB-1.0 could be observed.
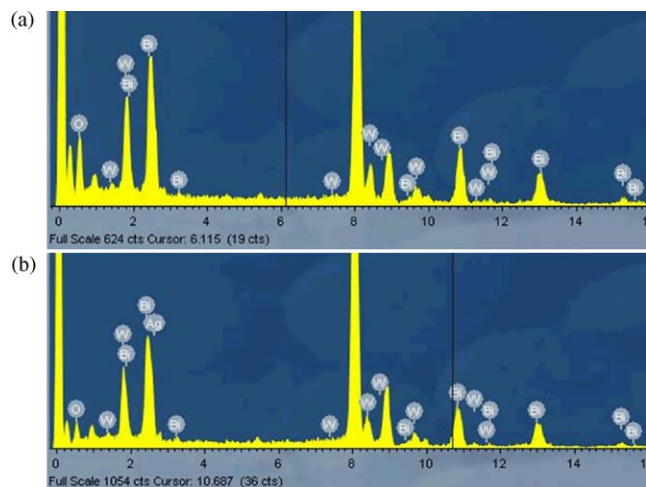
3.3. Diffuse reflectance UV–vis spectroscopy

The UV–vis diffuse reflectance spectrum (DRS) of the Ag-loaded Bi_2WO_6 sample is compared with that of pure Bi_2WO_6 in Fig. 4. The fundamental absorbance edge of Bi_2WO_6 (curve a) is about 450 nm due to the intrinsic band-gap transition [30]. The absorption curve of Ag-loaded Bi_2WO_6 (curve b and c) is obviously different from that of Bi_2WO_6. A broad absorption band centered at around 450 nm is visible, which indicates that it is silver metal not other compounds containing silver existed in the samples. The prominent absorption in the visible light region could be attributed to the surface plasmon band of Ag nanoparticles. The surface plasmon absorption in the metal nanoparticles arises from the collective oscillations of the free conduction band electrons that are enhanced by the incident electromagnetic radiation. And it is sensitive to particle sizes, shapes, the particle size distribution and the surrounding medium, etc. [31,32]. The plasmon absorption band of the small Ag nanoparticles prepared using borohydride reduction is around 380 nm. The red-shift in the plasmon absorption seen in the Ag-loaded Bi_2WO_6 sample might be related to the refractive index of the surrounding medium. It is obvious that a dampening and broadening surface plasmon band exhibits with the higher silver concentration, which could be ascribed to the increased size and size distribution of silver nanoparticles. The amount of silver initially present in the system determines the maximum particle size and size distribution, therefore influences the absorption of light. The effect of surface plasmon resonance
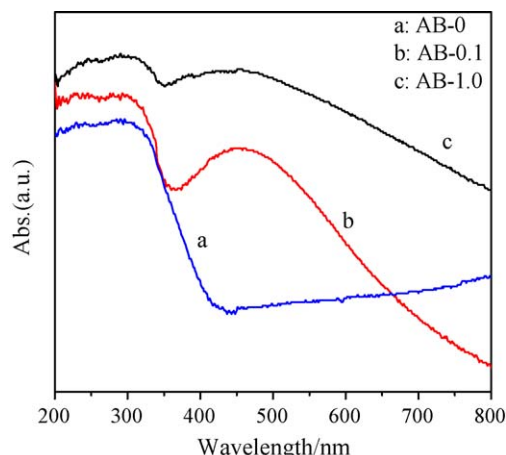

Fig. 3. EDX microanalysis spectra of the area with and without the silver deposited.

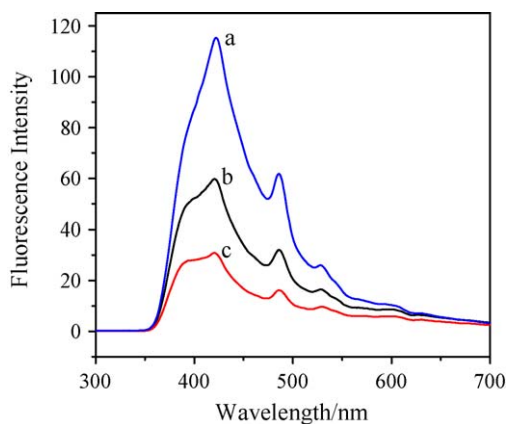**Fig. 4.** UV–vis absorption spectra of Bi_2WO_6 and Ag-loaded Bi_2WO_6.

Fig. 5. The room temperature photoluminescence (PL) spectra of Bi_2WO_6 (a), Ag-loaded Bi_2WO_6 (AB-0.75) (b) and Ag-loaded Bi_2WO_6 (AB-0.1) (c) (λ_{Ex} = 300 nm).

Fig. 6. The antibacterial efficiency of *E. coli* with Bi_2WO_6 and different contents of Ag-loaded Bi_2WO_6. AB-0.05, AB-0.1, AB-0.5, AB-0.75 and AB-1.0 are denoted according to the molar of reagent $AgNO_3$ used in the preparation (0.05, 0.1, 0.5, 0.75 and 1.0 mmol), AB-0 representatives Bi_2WO_6 without the deposition of Ag nanoparticles.

owing to Ag nanoparticles has a partial contribution to the enhanced photocatalytic antibacterial activity.

3.4. Photoluminescence spectra

Since photoluminescence (PL) emission arises from the recombination of free carriers, the PL spectra is subservient to investigate the migration, transfer, and recombination processes of the photogenerated electron-hole pairs in a semiconductor [33,34]. Fig. 5 shows the PL spectra of pure Bi_2WO_6 and Ag-loaded Bi_2WO_6 in the range of 300–700 nm excited by 300 nm. Bi_2WO_6 has a broad blue-green emission peak at 420–530 nm [35]. Three intense emission peaks appeared at 423, 485, and 528 nm, respectively in the spectra of pure Bi_2WO_6. There was a significant decrease in the intensity of PL spectra of Ag-loaded Bi_2WO_6 (AB-0.1) compared to that of pure Bi_2WO_6. A weaker intensity of the peak represents a lower recombination probability of free charges. It indicates that the noble metal Ag deposition could effectively inhibit the recombination of photogenerated charge carriers, which is helpful for the separation of photogenerated electron–hole pairs in Bi_2WO_6. Moreover, it can be observed that at higher Ag content, the peak intensities of sample AB-0.75 are stronger than that of sample AB-0.1. This can be ascribed to Ag deposits behaving as recombinant centers conversely.

3.5. Bacterial inactivation under visible light irradiation

The antibacterial activities of the Ag-loaded Bi_2WO_6 were exhibited by the killing effect of *E. coli* and *S. epidermidis*, which were evaluated through the decrease of the colony number formed on an agar plate. The bacteria with the absence of photocatalysts did not change before and after the visible light illumination for 0.5 h. The bacteria with Ag-loaded Bi_2WO_6 photocatalysts in the dark decreased at a low level due to the bactericidal effect of a small quantity of Ag. For comparison, the photocatalytic performance of the pure Bi_2WO_6 was also checked under the identical condition as that of Ag-loaded Bi_2WO_6. It is found that the metallic silver deposited on Bi_2WO_6 can notably enhance the photocatalytic activity in the disinfection of pathogenic bacteria when the Ag content is relatively lower, even eliminating the contribution of bactericidal effect brought by silver metal. After 0.5 h visible light irradiation, the bactericidal percentages of *E. coli* are 39%, 75%, and 99% in the presence of 0.5 mg/mL AB-0, AB-0.05, and AB-0.1, respectively (Fig. 6). The enhanced photocatalytic activities of the Ag-loaded Bi_2WO_6 can be explained by improved charge separation due to the loading of Ag content. When the Ag content is relatively higher, the photocatalytic activity of the Ag–Bi_2WO_6
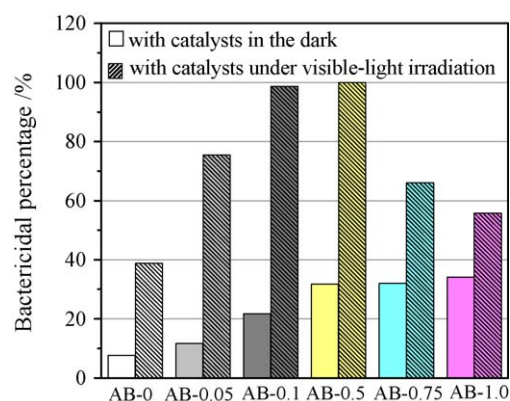
decreases with the increases of Ag content. Higher Ag deposits conversely behave as recombinant centers, encouraging the recombination of charge carriers. The effect of Ag deposits on the separation of photoinduced electrons and holes in Bi_2WO_6 photocatalysts has been confirmed by the PL spectra. The results show that there is an optimum loading level of Ag content. The element analyses of the Ag-loaded Bi_2WO_6 samples were operated through electron probe X-ray microanalyser (EPMA-8705QH2, Shimadzu, Japan) and energy dispersive-spectrometer (INCA Energy, Oxford Instruments, UK). The Ag atomic percentage of Ag deposited on the Bi_2WO_6 nanoparticles were 0, 0.72, 1.29, 4.90, 6.46 and 9.64 for the Ag-loaded Bi_2WO_6 samples AB-0, AB-0.05, AB-0.1, AB-0.5, AB-0.75 and AB-1.0, respectively. The sample AB-0.1 (1.29 at.%) exhibited the best photocatalytic activity eliminating the contribution of bactericidal effect brought by silver metal. The silver metal content have an obvious effect on the activity of the Ag-loaded Bi_2WO_6 catalysts.

To confirm the stability of the high photocatalytic performance of the Ag-loaded Bi_2WO_6 photocatalysts, the circulating runs in the photocatalytic inactivation of *E. coli* in the presence of AB-0.5 under visible light ($\lambda > 420$ nm) were checked. The photocatalytic activity did not exhibit any significant loss after five recycles for the photocatalytic inactivation of *E. coli* (Fig. 7). It indicates that the Ag-loaded Bi_2WO_6 photocatalyst have high stability during the bacteria inactivation.

S. epidermidis, a Gram-positive bacterium, was also inactivated efficiently by Ag-loaded Bi_2WO_6 (AB-0.1) under visible light
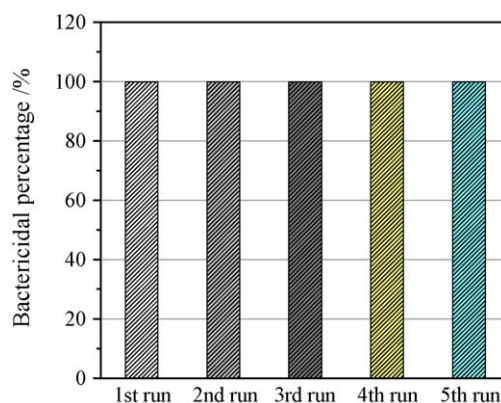

Fig. 7. Cycling runs in the photocatalytic inactivation of *E. coli* in the presence of AB-0.5 under visible light.
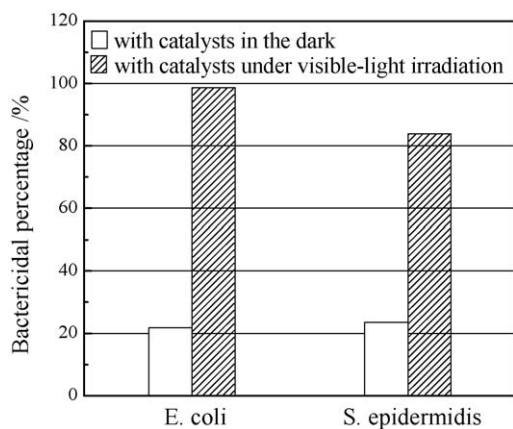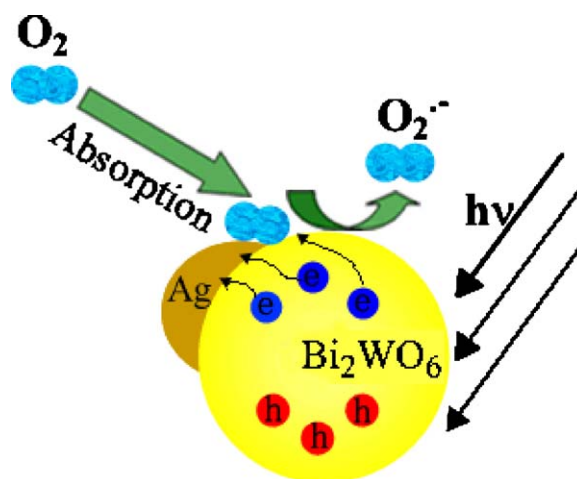
Fig. 8. The antibacterial efficiency of *E. coli*, a Gram-negative bacterium, and *S. epidermidis*, a Gram-positive bacterium with Ag-loaded Bi_2WO_6 (AB-0.1).

irradiation (Fig. 8). After 0.5 h visible light irradiation, the bactericidal percentage of *S. epidermidis* is 84% in the presence of 0.5 mg/mL AB-0.1, while 99% of *E. coli* is killed under otherwise identical conditions. Obviously, Ag-loaded Bi_2WO_6 shows higher bactericidal activity for *E. coli* than *S. epidermidis*, which could be attributed to the different structure of Gram-positive and Gram-negative cell walls. For *S. epidermidis*, a Gram-positive bacterium, the cell wall is composed of a 20–80 nm thick peptidoglycan layer. The subunits of peptidoglycan have a high degree of cross-linking and thus lead to forming a three-dimensional network configuration, which is tough, close connected, and high mechanical robustness. In contrast, the component and structure of cell wall of *E. coli*, a Gram-negative bacterium, is multilaminate and more complicated compared to Gram-positive bacterium. However, the cell wall is relatively loose and the thickness is only 10–15 nm. Hence the Gram-positive envelope affords better protection against the oxidative species produced during the photocatalytic process. This interpretation would account for the higher antibacterial activity of the Ag-loaded Bi_2WO_6 towards Gram-negative bacteria than Gram-positive bacteria. The electrostatic interaction between bacteria and photocatalysts might be also used to interpret this phenomenon [5].

3.6. Roles of Ag nanoparticles deposited on Bi_2WO_6

The photocatalytic activity of Bi_2WO_6 for inactivation of pathogenic bacteria is enhanced by the Ag loading arising from the following mechanisms: (i) Ag nanoparticles could act as electron traps to facilitate the separation of photogenerated electron-hole pairs and promotes interfacial electron transfer process; (ii) The surface plasmon resonance of Ag nanoparticles under visible light irradiation may enhance the photocatalytic activity of Bi_2WO_6.

A pathway of enhanced photocatalytic activity for bacterial inactivation with Ag-loaded Bi_2WO_6 is shown in Scheme 1. The photogenerated electrons excited to the conduction band of Bi_2WO_6 under visible light irradiation were entrapped by Ag nanoparticles due to its high Schottky barriers at the metal–semiconductor interface, and thus reduced the recombination possibility with photogenerated holes, which was confirmed by the photoluminescence spectra. The electrons could be scavenged by present molecular oxygen absorbed on the surface and produce the reactive oxygen radicals, while the valence hole photogenerated on the surface of Bi_2WO_6 could not react with OH^- or H_2O molecules to form $^{\bullet}OH$ radicals. Because the standard redox potential of the valence band is more negative than that of $^{\bullet}OH/OH^-$ [36]. The reactive oxygen radicals and the photogenerated

Scheme 1. Photocatalytic pathway for the *E. coli* inactivation on Ag-loaded Bi_2WO_6 nanoparticles.

holes are responsible for the inactivation of microorganisms. It is also proposed that appropriate contents of Ag deposition could increase the surface hydroxyl contents and thus improve the photocatalytic activity [37]. The noble metal clusters act as electron sink and thus promote charge separation in metal-deposited semiconductor particles. The process has been researched widely and demonstrated the picosecond dynamics of an interparticle electron transfer between semiconductor and metal nanoclusters [38].

In our study, the surface plasmon resonance band of Ag nanoparticles was obtained, so did the enhanced photocatalytic activity with Ag-loaded Bi_2WO_6. It is believed that the effect of surface plasmon resonance also contributes to the enhanced photocatalytic inactivation of pathogenic bacteria under visible light irradiation, considering the previous report of the enhanced photocatalytic activity owing to localized surface plasmon [20].

4. Conclusions

Noble metal Ag was deposited on Bi_2WO_6 via a facile alcohol-thermal process in ethylene alcohol system. The photocatalytic activity of Ag-loaded Bi_2WO_6 was greatly enhanced compared with pure Bi_2WO_6. Both Gram-negative and Gram-positive bacteria were inactivated efficiently by Ag-loaded Bi_2WO_6 under visible light irradiation. The content of silver has an impact on the catalytic activity of Ag-loaded Bi_2WO_6 photocatalyst. Synergetic effect of the noble metal and semiconductor is important for improving the performance of nanocomposites in photocatalytic applications. The study is helpful for the design of new photocatalysts with enhanced photocatalytic activity.

References

[1] T. Matsunaga, R. Tomada, T. Nakajima, H. Wake, FEMS Microbiol. Lett. 29 (1985) 211–214.
[2] Y. Lan, C. Hu, X. Hu, J. Qu, Appl. Catal. B: Environ. 73 (2007) 354–360.
[3] C. Hu, J. Guo, J. Qu, X. Hu, Langmuir 23 (2007) 4982–4987.
[4] C. Hu, Y. Lan, J. Qu, X. Hu, A. Wang, J. Phys. Chem. B 110 (2006) 4066–4072.
[5] C. Hu, X. Hu, J. Guo, J. Qu, Environ. Sci. Technol. 40 (2006) 5508–5513.
[6] H. Tada, K. Teranishi, Y. Inubushi, S. Ito, Langmuir 16 (2000) 3304–3309.

 [7] X.F. You, F. Chen, J.L. Zhang, M. Anpo, Catal. Lett. 102 (2005) 247–250.
 [8] F.B. Li, X.Z. Li, Appl. Catal. A: Gen. 228 (2002) 15–27.
 [9] I.M. Arabatzis, T. Stergiopoulos, D. Andreeva, S. Kitova, S.G. Neophytides, P. Falaras, J. Catal. 220 (2003) 127–135.
[10] W. Zhao, C. Chen, X. Li, J. Zhao, H. Hidaka, N. Serpone, J. Phys. Chem. B 106 (2002) 5022–5028.
[11] S.W. Lam, K. Chiang, T.M. Lim, R. Amal, G.K.C. Low, Appl. Catal. B 72 (2007) 363–372.
[12] S. Jin, F. Shiraishi, Chem. Eng. J. 97 (2004) 203–211.
[13] C.M. Wang, A. Heller, H. Gerischer, J. Am. Chem. Soc. 114 (1992) 5230–5234.
[14] M.A. El-Sayed, Acc. Chem. Res. 34 (2001) 257–264.
[15] (a) N.R. Jana, T.K. Sau, T. Pal, J. Phys. Chem. B 103 (1999) 115–121;
     (b) N. Pradhan, A. Pal, T. Pal, Langmuir 17 (2001) 1800–1802.
[16] V. Subramanian, E. Wolf, P. Kamat, J. Phys. Chem. B 105 (2001) 11439–11446.
[17] C.Y. Wang, C.Y. Liu, X. Zheng, J. Chen, T. Shen, Colloid Surf. A 131 (1998) 271–280.
[18] V. Vamathevan, R. Amal, D. Beydoun, G. Low, S. McEvoy, J. Photochem. Photobiol. A 148 (2002) 233–245.
[19] N. Chandrasekharan, P.V. Kamat, J. Phys. Chem. B 104 (2000) 10851–10857.
[20] K. Awazu, M. Fujimaki, C. Rockstuhl, J. Tominaga, H. Murakami, Y. Ohki, N. Yoshida, T. Watanabe, J. Am. Chem. Soc. 130 (2008) 1676–1680.
[21] Y. Shi, S. Feng, C. Cao, Mater. Lett. 44 (2000) 215–218.
[22] A. Kudo, S. Hijii, Chem. Lett. 28 (1999) 1103–1104.
[23] J. Tang, Z. Zou, J. Ye, Catal. Lett. 92 (2004) 53–56.
[24] C. Zhang, Y. Zhu, Chem. Mater. 17 (2005) 3537–3545.
[25] L. Wu, J. Bi, Z. Li, X. Wang, X. Fu, Catal. Today 131 (2008) 15–20.
[26] L.S. Zhang, W.Z. Wang, L. Zhou, H.L. Xu, Small 3 (2007) 1618–1625.
[27] M. Shang, W. Wang, S. Sun, L. Zhou, L. Zhang, J. Phys. Chem. C 112 (2008) 10407–10411.
[28] M. Shang, W. Wang, H. Xu, Cryst. Growth Des. 9 (2009) 991–996.
[29] P. Claus, H. Hofmeister, J. Phys. Chem. B 103 (1999) 2766–2775.
[30] A. Kudo, I. Tsuji, H. Kato, Chem. Commun. 17 (2002) 1958–1959.
[31] P. Mulvaney, Langmuir 12 (1996) 788–800.
[32] S. Link, M.A. El-Sayed, J. Phys. Chem. B 103 (1999) 8410–8426.
[33] F.B. Li, X.Z. Li, Chemosphere 48 (2002) 1103–1111.
[34] F.B. Li, X.Z. Li, Appl. Catal. A 228 (2002) 15–27.
[35] Q. Xiao, J. Zhang, C. Xiao, X.K. Tan, Catal. Commun. 9 (2008) 1247–1253.
[36] H.B. Fu, C.S. Pan, W.Q. Yao, Y.F. Zhu, J. Phys. Chem. B 109 (2005) 22432–22439.
[37] W. Lu, S. Gao, J. Wang, J. Phys. Chem. C 112 (2008) 16792–16800.
[38] P.V. Kamat, B. Shanghavi, J. Phys. Chem. B 101 (1997) 7675–7679.